Structure and energetics of stoichiometric TiO_2 anatase surfaces

Michele Lazzeri,[1] Andrea Vittadini,[2] and Annabella Selloni[1]
[1]*Department of Chemistry, Princeton University, Princeton, New Jersey 08540*
[2]*CSSRCC-CNR, via Marzolo 1, I-35131 Padova, Italy*
(Received 15 November 2000; published 26 March 2001)

We present an *ab initio* density-functional investigation of the structure and energetics of several stoichiometric 1×1 low-index surfaces of anatase, a TiO_2 polymorph $\sim9\%$ less dense and ~1.2 kcal/mol less stable than rutile. Although our calculations do not reproduce the relative ordering of the two phases that is observed experimentally, the calculated bulk structural and elastic properties of both polymorphs are in excellent agreement with the experiment, suggesting that surface relaxations are correctly described as well. As expected, the surface energies of anatase appear to be related to the presence of undercoordinated Ti atoms: the surfaces with fourfold-coordinated Ti atoms have a larger energy than those with fivefold-coordinated Ti. Furthermore, we find that the average surface energy of a TiO_2 anatase macroscopic crystal is smaller than that of rutile. Finally, patterns in the relaxation of the surface atoms which are common to different surfaces are analyzed.

DOI: 10.1103/PhysRevB.63.155409 PACS number(s): 68.03.Cd, 68.35.Bs, 71.15.Nc, 71.15.Mb

I. INTRODUCTION

Anatase is a TiO_2 polymorph which is less stable than rutile, but more efficient than rutile for several applications, including catalysis,[1] photocatalysis,[2] and, especially, dye-sensitized solar cells.[3] In all these applications, surface properties are of major importance. However, while the surfaces of rutile have been extensively investigated,[2,4] due to the limited availability of sufficiently large anatase single crystals the fundamental surface properties of this polymorph are still largely unexplored. Only very recently, thanks to improved sample preparation techniques, have experimental studies of well defined anatase surfaces started to appear.[5,6]

Motivated by these advances, and following a preliminary study of the (101) and (001) surfaces by two of us,[7] we have carried out an extensive first-principles investigation of the structure and energetics of several stoichiometric 1×1 anatase surfaces. Besides studying (101) and (001) surfaces in much greater detail, we also consider (100), (110), and (103) terminations. All these surfaces are exposed by TiO_2 nanocrystals obtained by typical, e.g. sol-gel, procedures,[8,9] the (101) surface also being the one mainly exposed by natural anatase samples.

The only previous theoretical study of clean anatase surfaces of which we are aware is an atomistic simulation based on empirical interatomic potentials.[10] An interesting point suggested by the results of this study is that the surface energies of anatase may be smaller than those of the rutile phase. This is important, since a surface energy difference of this type can explain the fact that experimentally crystalline TiO_2 nanoparticles are found to ''prefer'' the anatase structure for diameters up to about 10 nm, transforming to the rutile structure only after growing above a certain size.[11] In order to confirm this explanation, a careful evaluation of the relative surface energies of rutile and anatase is required. Therefore, in this work we shall extend our calculations to the rutile (110) surface, which is known to be the most stable one for this TiO_2 polymorph.[12] By considering surface energies calculated with the same technical ingredients, we expect the comparison to be more meaningful.

The layout of this paper is as follows. As we are interested in comparing the surface energies of anatase and rutile, we start (Sec. II) by studying the bulk structural properties and cohesive energies of both polymorphs. In Sec. III, after describing some details of our surface calculations, we discuss the energies of the various anatase surfaces. The relaxation patterns of the different structures are analyzed in Sec. IV. Concluding remarks are presented is Sec. V.

II. BULK PROPERTIES OF THE RUTILE AND ANATASE PHASES

Rutile and anatase (see Fig. 1) are the two most common and widely used polymorphs of TiO_2. Both crystals are formed by chains of distorted TiO_6 octahedra, and their tetragonal structure can be described in terms of three parameters: two cell edges a and c, and one internal parameter d. In the most stable rutile phase the unit cell contains two TiO_2 units. Each Ti atom is coordinated to the six neighboring oxygens via two (long) apical and four (short) equatorial bonds, of lengths 1.976 and 1.946 Å, respectively, at 15 K.[13] Each O atom is coordinated to three Ti atoms via one long bond and two short bonds, lying in the same plane. The metastable anatase phase is $\sim9\%$ less dense than rutile, and has a tetragonal unit cell containing four TiO_2 units. The

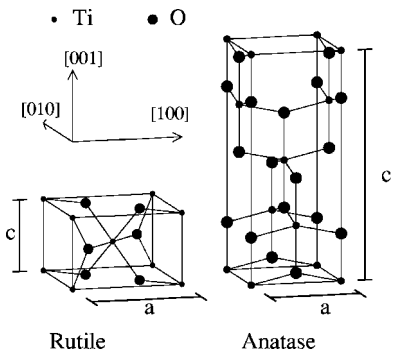

FIG. 1. Bulk TiO_2 crystal structure in the rutile and anatase phases. The space groups are $P4_2/mnm$ and $I4_1/amd$, respectively.

TABLE I. Comparison between calculated structural properties of the rutile and anatase phases, with experimental data (expt). The quantities are described in the text. The difference between calculated and measured values of the three parameters defining the structure are shown as a percentage in parentheses. Calculations were performed using three different approximations for the exchange-correlation functional: PBE, LDA, and BLYP (see the text).

	a (Å)	c (Å)	d (Å)	B_0 (GPa)	B_0'	E^{coh} (eV/TiO_2)
			Rutile			
expt:	4.587[a]	2.954[a]	1.976[a]	211±10[b]	6.5±0.7[b]	19.9[c]
PBE:	4.634(+1.0%)	2.963(+0.3%)	1.999(+1.2%)	204	4.62	21.44
LDA:	4.546(−0.9%)	2.925(−1.0%)	1.952(−1.2%)	249	4.98	24.44
BLYP:	4.679(+2.0%)	2.985(+1.0%)	2.021(+2.3%)	200	5.27	20.27
			Anatase			
expt:	3.782[a]	9.502[a]	1.979[a]	179±2[d]	4.5±1.0[d]	
PBE:	3.786(+0.1%)	9.737(+2.5%)	2.002(+1.2%)	176	2.99	21.54
LDA:	3.735(−1.2%)	9.534(+0.3%)	1.973(−0.3%)	199	1.72	24.46
BLYP:	3.828(+1.2%)	9.781(+2.9%)	2.014(+1.8%)	178	2.36	20.39

[a]Low temperature data from Ref. 13.
[b]Data from Ref. 31.
[c]Data from Ref. 33.
[d]Data from Ref. 35.

coordination of Ti and O atoms is the same as in rutile; however, the octahedra are significantly more distorted, with apical and equatorial bonds of 1.979 and 1.932 Å, respectively.[13]

Calculations were performed using a plane-wave pseudopotential approach within density-functional theory (DFT). Three different approximations were used for the exchange-correlation functional: one local, i.e., the local density approximation (LDA),[14] and two gradient-corrected, i.e., the Perdew-Burke-Ernzerhof (PBE)[15] and Becke-Lee-Yang-Parr (BLYP)[16] functionals. The performance of these functionals for the description of various molecular and solid-state systems is currently a subject of great interest (see, e.g., Ref. 17). While the BLYP functional can be very accurate for atoms and molecules, the PBE functional is usually the most reliable, since it performs well for both small and extended systems. Instead, the LDA typically provides good structural properties, but overestimates binding energies.

For both oxygen and titanium, electron-core interactions are described by ''ultrasoft'' pseudopotentials.[18] For each different exchange-correlation functional, a consistent pseudopotential was used. Valence states include $2s$ and $2p$ shells for O (six electrons), and $3s$, $3p$, $3d$, and $4s$ states for Ti (12 valence electrons). The smooth part of the wave functions is expanded in plane waves, with a kinetic-energy cutoff of 25 Ry, while the cutoff for the augmented electron density is 200 Ry. For rutile (anatase) a $4\times4\times4$ ($4\times4\times2$) mesh of k points was used to sample the Brillouin zone.

To determine the structural properties of the two phases, the crystal total energies were calculated on a grid of points in the three-dimensional (a,c,d) parameter spaces (in both the rutile and anatase cases, d indicates the Ti-O apical distance). The minimum-energy configurations were obtained by interpolation and are compared to low-temperature experimental data in Table I. The bulk modulus B_0, and its derivative B_0', given in this table, are obtained via a third-order Birch-Murnaghan[19] equation of state, while the cohesive energies (E^{coh}, obtained as the difference between the total energy of the system and the sum of the energies of the isolated atoms) include a spin-polarized correction for the isolated atoms.[20]

From Table I we can see that the agreement between theory and experiment is very good for what concerns the structural parameters and the bulk modulus, particularly when the PBE or LDA exchange-correlation functional are used. According to our calculations, however, the anatase phase is more stable than rutile, whereas experimentally rutile is the most stable, by $\sim$1.2–1.5 kcal/mol.[21,22] Within the LDA, the difference in cohesive energy between anatase and rutile is only 0.02 eV/TiO_2, while it is 0.10 and 0.12 eV/TiO_2 with PBE and BLYP, respectively. No significant variation in the relative cohesive energies of the two phases is found if these are calculated using the experimental lattice parameters, instead of the theoretically optimized ones, or if a higher-energy cutoff and a larger number of k points are used. This suggests that the discrepancy between our calculations and experiment is unlikely to originate from computational inaccuracies. Furthermore, yet unpublished all-electron LDA calculations by Cangiani *et al.*, within the linearized-augmented-plane-wave method, found results very similar to ours,[23] indicating that our discrepancy with experiment is not related to the pseudopotentials we use.

So far there have been very few theoretical first-principles studies where the relative stability of rutile and anatase was directly compared. The correct ordering of the two phases was obtained in a LDA study by Dewhurst and Lowther,[24] who optimized their structures with respect to a, while constraining the ratios c/a and d/c. Instead, a discrepancy similar to ours, i.e., anatase more stable than rutile, was also found in a Hartree-Fock calculation by Fahmi *et al.*[25] These

authors, however, found that, by adding correlation in a post-self-consistent field step through the Colle-Salvetti[26] functional, the correct ordering of the two phases could be obtained. They also pointed out that the correlation effects are more important for the denser rutile structure than for anatase. This is not inconsistent with our results. Table I indeed shows that, with the LDA (BLYP) functional, which favors denser (less dense) phases, the disagreement with the experiment decreases (increases).

III. SURFACE ENERGIES

A. Computational details

Surface calculations were performed using both the PBE (Ref. 15) and the LDA (Ref. 14) exchange-correlation functionals (BLYP was not used, as test calculations indicate that this functional is less accurate for surfaces[17]). We used two low-symmetry k points in the irreducible surface Brillouin zone for all surfaces but the (001), for which four points were considered. The periodically repeated slabs were separated one from the other by a vacuum region ~ 9 Å wide, and the theoretical lattice constant was used. Other geometrical features, the number of layers and number of atoms in the slab, are summarized in Table II. The positions of all the atoms of the slab were relaxed using a damped Car-Parrinello molecular dynamics,[27] until residual forces were less than 0.02 eV/Å. The two relaxed surfaces of the slab turn out to be always equivalent. Thus the surface energy is calculated as the difference between the total energy of the slab and the total energy of an equal number of TiO_2 units in the bulk phase, divided by the total exposed area.

In order to make a direct comparison with rutile, we also calculated the surface energy of the relaxed (110) surface of the rutile phase. Our LDA value (0.84 J/m^2) agrees closely with the calculation of Ref. 12 (0.83 J/m^2 for a six-layer relaxed structure). Assuming that a similar agreement also holds for the energies of the other rutile surfaces, we shall compare our LDA surface energies for anatase with the rutile results of Ref. 12.

B. Wulff construction

On the stoichiometric low-index surfaces that we examine, both undercoordinated Ti and O atoms are present. The latter are always in the form of twofold-coordinated oxygens. Fivefold-coordinated Ti atoms are found on the (001), (101), and (100) surfaces, as well as on one of the two possible terminations of the (103) surface. Fourfold Ti atoms are exposed on the other (103) termination, and on the (110) surface.

The energies of the various surfaces, both before and after relaxation, are reported in Table II. Similarly to what was found for rutile surfaces,[28] values calculated with the LDA are systematically larger than those obtained with the PBE functional, by ~ 0.40 J/m^2. Although the LDA is known to be substantially less accurate than the PBE for describing the cohesion in molecules and solids, there are indications that it might perform better than the PBE for the calculation of surface energies.[29,30] At present, because of the lack of accurate measurements to compare with, and because of the larger error of the PBE with respect to the LDA in the relative bulk energies of the rutile and anatase phases, it is not clear which functional is more reliable for describing surface properties. However, if we assume that the error due to the exchange and correlation functional is systematic to all the surfaces (that is, it does not greatly affect the relative energies of two different surfaces), it is still possible to extract some trends from our results. It is apparent that the relaxation of atoms on the surface contributes significantly to the calculated surface energies. As expected, surface energies appear to be related to the presence of undercoordinated Ti atoms. The results shown in Table II indicate that surfaces with fourfold-coordinated Ti have a larger energy than those with fivefold-coordinated Ti. Furthermore, the surface energy (of the relaxed structure) approximately increases with the increase of the density of undercoordinated Ti atoms.

The shape of a thermodynamically stable macroscopic crystal is given by the standard Wulff construction,[34] which can be done as follows. Knowing the surface energy $E^{surf}(\hat{\mathbf{n}})$ for every direction $\hat{\mathbf{n}}$, one should draw a plane perpendicular to $\hat{\mathbf{n}}$, passing through the point having a distance

TABLE II. Formation energies of various surfaces, calculated in this work. The ''faceted'' and ''smooth'' terminations of the (103) surface are denoted $(103)_f$ and $(103)_s$, respectively. In the left panel, N_{lay} is the number of Ti layers and N_{at} is the total number of atoms. In the central panels, the surface energies for the unrelaxed (E^{unrl}) and relaxed structures (E^{rel}), calculated with PBE and LDA functionals (see the text), are reported. Surface energies in parentheses, calculated for thinner slabs, are less reliable. In the rightmost panel, the surface densities of fivefold- and fourfold-coordinated Ti atoms [nTi(5) and nTi(4), respectively] are reported.

	N_{lay}	N_{at}	E^{unrl}_{PBE} (J/m^2)	E^{rel}_{PBE} (J/m^2)	E^{unrl}_{LDA} (J/m^2)	E^{rel}_{LDA} (J/m^2)	nTi(5) (10^{-2} Å^{-2})	nTi(4) (Å^{-2})
Rutile								
(110)	6	36	1.38	0.35	1.78	0.84	5.3	
Anatase								
(101)	6	36	1.28	0.49	1.56	0.84	5.1	
(101)	4	24		(0.45)			'' ''	
(100)	6	36	1.59	0.58	1.90	0.96	5.4	
(100)	4	24		(0.63)			'' ''	
(001)	6	18	1.12	0.98	1.46	1.38	7.0	
(001)	4	12		(0.98)			'' ''	
$(103)_f$	8	48	1.50	0.90			7.1	
$(103)_f$	6	36		(0.89)			'' ''	
$(103)_s$	8	48	2.40	0.99				3.5
$(103)_s$	6	36		(0.99)				'' ''
(110)	7	42	2.17	1.15				3.8
(110)	6	36		(1.05)				'' ''

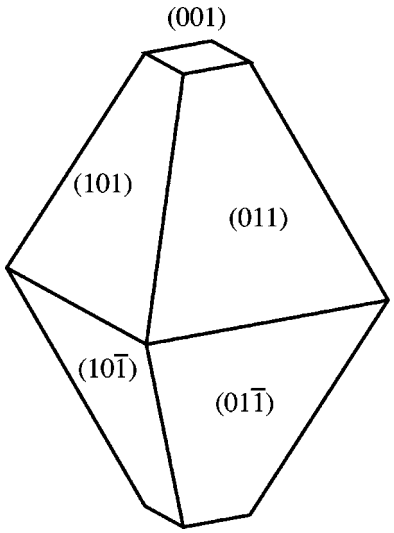

FIG. 2. The equilibrium shape of a TiO_2 crystal in the anatase phase, according to the Wulff construction and the calculated surface energies of Table II.

from the origin of magnitude $E^{surf}(\hat{\mathbf{n}})$. The Wulff construction is the inner envelope of all the planes corresponding to every $\hat{\mathbf{n}}$ direction. Figure 2 shows the Wulff construction for anatase, according to the energies of Table II (the construction does not essentially change whether we use LDA or PBE energies).

In agreement with experimental observations for naturally occurring anatase,[32] our Wulff construction shows that in anatase crystals the only two surfaces exposed to the vacuum are the (101) and (001) surfaces. The most stable (101) surface is the one mainly exposed, and constitutes more than 94% of the crystal surface. For rutile, instead, three different surfaces are exposed, (110), (101), and (100), and, according to the LDA surface energies in Ref. 12, the most stable (110) termination forms $\sim$56% of the total surface exposed. In anatase the average surface energy for a macroscopic crystal (defined as the sum of the energies of the exposed surfaces, weighted with the corresponding area in the Wulff construction) is 0.90 J/m^2, within the LDA, and 0.53 J/m^2, using the PBE functional. The analogous quantity for rutile, calculated using the LDA data from,[12] is 1.09 J/m^2, i.e., $\sim$20% larger than our LDA value for anatase. Given the consistency between our LDA calculations and those of Ref. 12 (see Sec. III A), it is safe to conclude that the calculated surface energy of anatase is indeed smaller than that for the rutile phase.

IV. SURFACE STRUCTURES

In this section we analyze the atomic relaxations on the anatase surfaces. Calculations for the (101), (100), and (001) surfaces were performed using both the LDA and PBE functionals, while only the latter was used for all other terminations. Since atomic positions obtained with the two functionals are essentially the same (except for a few cases that will be explicitly outlined), only the results obtained with the PBE functional are reported.

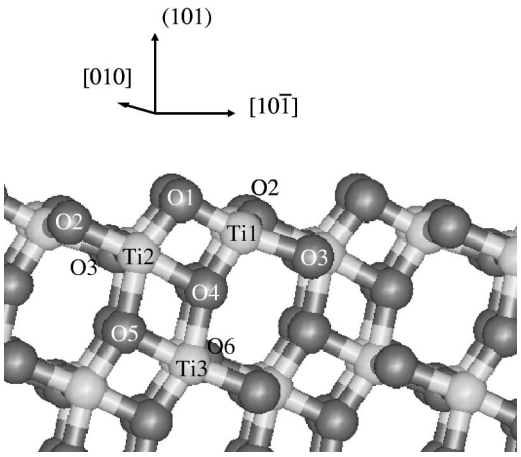

FIG. 3. The structure of the relaxed stoichiometric (101) surface. Equivalent atoms have the same label.

The relaxed surfaces show a complex structure. In what follows we shall try to identify features in the relaxation pattern that are common to more than one surface. These features concern the oxygen atoms at the surface, that, obviously, show a different behavior according to their coordination. Furthermore, undercoordinated oxygens show a different relaxation according to the Ti-O-Ti angle they form with the neighboring atoms. In the anatase bulk each oxygen and its three neighboring Ti atoms form a planar T-shaped structure, with an angle $\delta = 101.9^{o}$ between one apical bond and one equatorial bond, and $\theta = 156.2^{o}$ between the two equatorial bonds (our θ correspond to 2θ in the notation of Ref. 26). In what follows we will refer to these two angles as δ and θ.

A. (101) surface

The (101) surface is very corrugated, with a characteristic sawtooth profile perpendicular to the [010] direction (see Fig. 3). On it, both fivefold- and sixfold-coordinated Ti atoms are present (denoted Ti1 and Ti2 in Fig. 3, respectively), as well as twofold and threefold oxygens (O1 and O2, respectively). Calculated relaxations of some surface atoms are reported in Table III.

The most important outward relaxations are those of the fully coordinated Ti2 and O2 ($\sim$0.2 Å), while the undercoordinated Ti1 is displaced inward by ~ -0.2 Å. Each bridging oxygen (O1) is bonded to one Ti1 atom and one Ti2 atom (via an apical bond and an equatorial bond, respectively) forming a Ti-O-Ti δ-angle of 102^{o}. The O1 atom shows a lateral displacement along [10$\bar{1}$], that, together with the inward/outward relaxation of the neighboring titania, leads to a substantial tightening of O1 bonds. Finally, on the relaxed surface, the fully coordinated O2 atoms are located above the Ti1 atoms (they are below the Ti1 atom on the ideal surface). The corresponding O-Ti-O-Ti rings parallel to the surface become slightly twisted [the dihedral angle with the plane (100) is $\sim 8^{o}$], while the distance between oxygen atoms in these rings increases from $\sim$2.47 (ideal value) to

TABLE III. Structure of the relaxed (101) surface. Atom labels refer to Fig. 3. The left panel shows the atomic displacements from the bulk-truncated ideal positions, along three orthogonal directions. The right panel shows the expansion of the bonds between nearest neighbors, as a percentage from the bulk corresponding value. Apical (equatorial) bonds are indicated with *a* (*e*), and are 2.002 Å (1.942 Å). Displacements in parentheses are obtained with the LDA; all the others are obtained with the PBE.

Atomic displacements (Å)				Bond expansion		
Label	$[10\bar{1}]$	[010]	(101)	Label	Type	%
O1	0.29	0.00	−0.02	Ti1-O1	*a*	−8.6
O2	0.16	0.00	0.19	Ti1-O2	*e*	+2.0
	(0.17)		(0.15)	Ti1-O3	*a*	+3.3
				Ti1-O4	*e*	−8.4
O3	0.17	0.00	0.06	Ti2-O1	*e*	−5.0
O4	0.15	0.00	−0.07	Ti2-O2	*a*	+0.3
O5	0.06	0.00	0.04	Ti2-O3	*e*	−0.3
O6	−0.02	0.00	−0.04	Ti2-O4	*a*	+5.1
				Ti2-O5	*e*	+8.7
Ti1	0.02	0.00	−0.18	Ti3-O4	*e*	+5.2
Ti2	0.17	0.00	0.20	Ti3-O5	*a*	−1.2
Ti3	−0.04	0.00	−0.14	Ti3-O6	*e*	+0.0

~2.50 Å. This feature is also present in the structure calculated with the LDA, even if it is somewhat less marked (see Table III).

B. (100) surface

On the (100) surface (see Fig. 4), the outermost Ti atoms (T10 and T11) are fivefold coordinated, but sixfold-coordinated Ti atoms of the second layer (T20 and T21), which lie at the bottom of grooves along the [010] direction, are also exposed. Moreover, both twofold (O12 and O13) and threefold (O10 and O11) coordinated oxygens are present on the surface. Calculated relaxations of some surface atoms are reported in Table IV.

TABLE IV. Structure of the relaxed (100) surface. Atom labels refer to Fig. 4; also see the caption of Table III.

Atomic displacements (Å)				Bond expansion		
Label	[001]	$[0\bar{1}0]$	(100)	Label	Type	%
O10	0.04	0.00	0.18	T10-O12	*a*	−8.6
O11	−0.04	0.00	0.18	T10-O10	*a*	+4.6
O12	0.16	0.00	0.02	T10-O11	*e*	+1.2
O13	−0.16	0.00	0.02	T10-O21	*e*	−7.8
O20	−0.13	0.00	−0.03	T20-O12	*e*	−5.1
O21	0.13	0.00	−0.03	T20-O21	*a*	+6.7
O22	−0.01	0.00	0.10	T20-O23	*a*	+0.1
O23	0.01	0.00	0.10	T20-O22	*e*	+0.2
T10	−0.02	0.00	−0.16			
T11	0.02	0.00	−0.16			
T20	0.01	0.00	0.17			
T21	−0.01	0.00	0.17			

The fully coordinated O11 and O10 oxygens show an important outward relaxation (~0.2 Å), while the fivefold- and sixfold-coordinated exposed Ti atoms relax inward and outward, respectively. The twofold-coordinated oxygens are bonded to one fivefold-coordinated Ti atom and one sixfold-coordinated Ti atom, forming a Ti-O-Ti δ-angle of 103° (nearly the same as the ideal unrelaxed value), and both Ti-O bonds are shorter after the relaxation. This relaxation pattern is qualitatively similar to that of the (101) surface. Also in this case the fully coordinated oxygen atoms relax outward, while the structure is rearranged so as to tighten the bond of the undercoordinated oxygen. We do not observe a significant difference between PBE and LDA calculated structures, even if the energetics are different (see Sec. III).

C. (001) surface

On the (001) surface (see Fig. 5), fivefold-coordinated Ti atoms are present (denoted Ti1 in Fig. 5), as well as twofold- and threefold-coordinated oxygens (O1 and O2, respectively). Calculated relaxations of some surface atoms are reported in Table V.

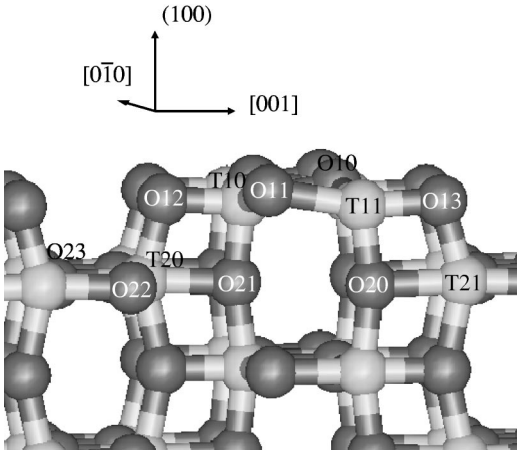

FIG. 4. The structure of the relaxed stoichiometric (100) surface.

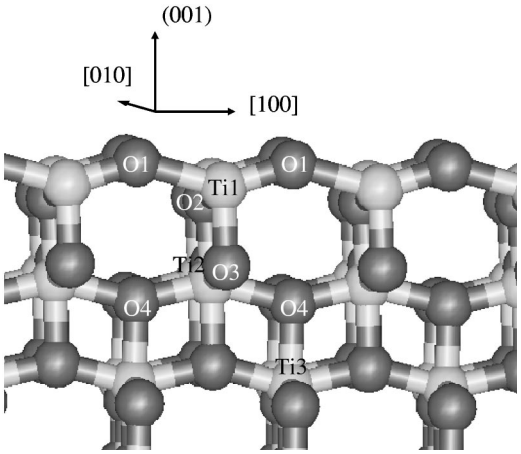

FIG. 5. The structure of the relaxed stoichiometric (001) surface.

TABLE V. Structure of the relaxed (001) surface. Atom labels refer to Fig. 5; also see the caption of Table III. On the relaxed surface, the bonds between the atom labeled Ti1 and its two nearest neighbors O1 are not equivalent, and are indicated with e^*. Results in parentheses are obtained with the LDA; all the others are obtained with the PBE.

Atomic displacements (Å)				Bond expansion		
Label	[100]	[010]	(001)	Label	Type	%
O1	−0.19	0.00	0.08	Ti1-O1	e^*	+13.4(9.0)
	(−0.13)		(0.04)	Ti1-O1	e^*	−9.5(−6.4)
				Ti1-O2	e	+0.1
O2	−0.17	0.00	−0.02	Ti1-O3	a	−3.4
	(−0.13)		(−0.02)	Ti2-O2	a	−1.2
				Ti2-O3	e	+0.1
O3	0.11	0.00	0.01	Ti2-O4	e^*	+1.9(1.0)
	(0.07)		(0.01)	Ti2-O4	e^*	−1.6(−0.7)
				Ti3-O4	a	−0.1
O4	0.02	0.00	−0.00			
Ti1	0.04	0.00	−0.06			
Ti2	−0.01	0.00	0.01			
Ti3	0.02	0.00	0.00			

On the ideal surface, the O1 bridging oxygens are bonded to the undercoordinated Ti1 via two equatorial bonds, forming a Ti1-O1-Ti1 θ angle. In the relaxed surface, the mirror plane symmetry along the [100] direction is broken: the two O1-Ti1 bonds become strongly inequivalent, with bond lengths of 2.20 and 1.76 Å, while the Ti-O-Ti θ angle is reduced to 146°. This symmetry breaking is obtained also with the LDA, even though the inequivalence of the two O1-Ti1 bonds is less pronounced (bond lengths of 2.08 and 1.80 Å). Furthermore, the O-Ti-O-Ti rings, perpendicular to the surface, that contain the fully coordinated O2 and O3 atoms, become slightly skewed [the dihedral angle with the plane (100) is ~6°], and the distance between O2 and O3 atoms is 2.46 Å (nearly the ideal value).

D. (103) surfaces

The stoichiometric (103) surface has two possible terminations, that we shall call ''faceted'' $(103)_f$ and ''smooth'' $(103)_s$. The $(103)_f$ termination has a sawtooth profile along the $[30\bar{1}]$ direction, so that (001) and (100) microfacets are exposed (see Fig. 6). The relaxations of some surface atoms are reported in Table VI. Ti atoms exposed to the vacuum are both fivefold coordinated (Ti1 and Ti2), and sixfold coordinated (Ti3). There are two inequivalent twofold-coordinated oxygens: O1 and O2. O1 is bonded to the two undercoordinated Ti1 and Ti2 atoms, forming a Ti-O-Ti δ angle of 99° (against an ideal value of 102°). Similarly to what was found on the (101) and (100) surfaces, both Ti-O1 bonds are contracted. On the other hand, the relaxation of O2, which is bonded to two undercoordinated Ti1 atoms forming a Ti-O-Ti θ-angle of 148° (against an ideal value of 156°), is similar to that of the undercoordinated oxygen on the (001) surface. In fact, the two Ti1-O2 bonds, which are equivalent in the ideal structure, become strongly inequivalent in the relaxed structure (bond lengths of 2.15 and 1.78 Å). Finally, as on the (101) and (100) surfaces, the fully coordinated oxygen (O3) undergoes an important outward relaxation (~0.2 Å). Also in this case the O-Ti-O-Ti rings (containing O3, Ti2, O6, and Ti3) become slightly skewed [the dihedral angle with the plane (100) is ~6.5°], while the distance between oxygen atoms in these rings increases to ~2.51 Å.

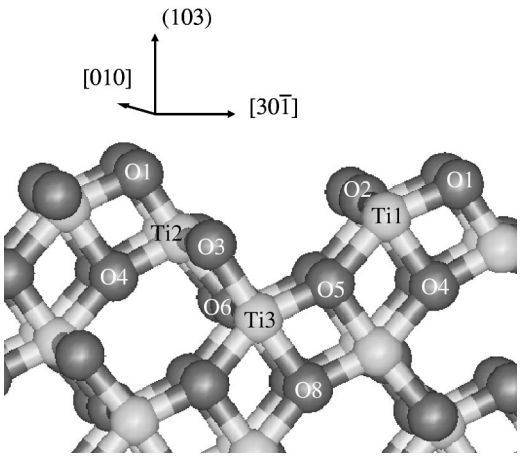

FIG. 6. The structure of the relaxed stoichiometric ''faceted'' termination of the (103) surface (see the text).

The ''smooth'' termination of the (103) surface (see Fig. 7) shows both fourfold- (Ti1) and sixfold-coordinated Ti atoms (Ti2 and Ti3). In addition, there are two inequivalent twofold-coordinated oxygens, denoted O3 and O2 in Fig. 7. O3 is bonded to the two fully coordinated Ti3 and Ti2 atoms, and it forms a Ti-O-Ti δ angle. In the relaxed structure (see Table VII), both bonds are contracted and the angle is 102°. O2 is bonded to the fully coordinated Ti3 atom and to the

TABLE VI. Structure of the ''faceted'' termination of the (103) surface. Atom labels refer to Fig. 6; also see the caption of Table III. On the relaxed surface, the bonds between the atom labeled Ti1 and its two nearest neighbors O2 are not equivalent, and are indicated with e^*.

Atomic displacements (Å)				Bond expansion		
Label	$[30\bar{1}]$	[010]	(103)	Label	Type	%
O1	0.20	0.03	−0.11	Ti1-O1	e	−3.0
O2	0.11	0.10	0.02	Ti1-O2	e^*	10.8
O3	0.20	0.00	0.18	Ti1-O2	e^*	−8.1
O4	0.08	−0.07	−0.08	Ti1-O4	a	−1.7
O5	0.07	0.04	−0.03	Ti1-O5	e	+5.6
O6	0.05	0.00	−0.02	Ti2-O1	a	−10.3
O7	−0.01	0.00	0.00	Ti2-O3	e	+1.7
O8	−0.00	0.00	−0.06	Ti2-O4	e	−7.1
				Ti2-O6	a	+3.1
Ti1	0.22	−0.09	−0.01	Ti3-O3	a	+0.2
Ti2	−0.08	0.00	−0.06	Ti3-O5	e	−3.0
Ti3	0.09	0.00	0.08	Ti3-O6	e	−0.4
Ti4	−0.09	0.00	−0.11	Ti3-O8	a	+2.7

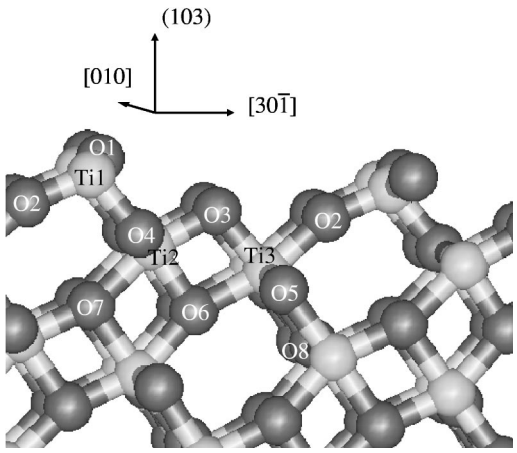

FIG. 7. The structure of the relaxed stoichiometric ''smooth'' termination of the (103) surface (see the text). The Ti2-O1 bond has the largest expansion, and the corresponding ''stick'' is deleted from the figure.

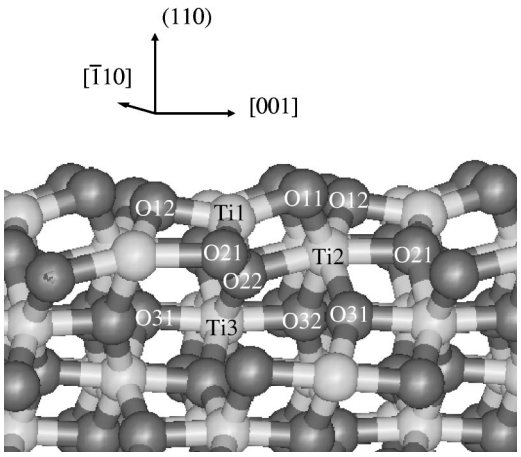

FIG. 8. The structure of the relaxed stoichiometric (110) surface.

undercoordinated Ti1 atom via two equatorial bonds, forming a Ti-O-Ti θ angle. In the relaxed structure the Ti1-O2 bond is contracted by $\sim$11%, while the Ti3-O2 bond is nearly ideal. The Ti-O-Ti θ-angle is 162°, larger than its ideal value. The fully coordinated O1 atoms undergo a huge outward relaxation, 0.5 Å, while the Ti2-O1 bond is expanded by $\sim$28%.

E. (110) surface

The (110) surface is shown in Fig. 8, and the relaxations of some surface atoms are reported in Table VIII. The atoms exposed to the vacuum are a fourfold-coordinated Ti atom and two twofold-coordinated oxygens of the first layer, as well as a fully coordinated oxygen of the second layer. In the ideal bulk truncated surface the atoms of the first layer are grouped in linear O-Ti-O units, parallel to the [001] direction, and arranged in a centered rectangular array. In the relaxed structure the oxygens of the first layer (denoted O11 and O12 in Fig. 8) display different displacements from the equilibrium positions, and are no longer equivalent. The two bonds of the O-Ti-O units of the first layer are both contracted, and the O-Ti-O angle is reduced to 147°.

F. Trends

Recurrent features in the relaxation patterns of the various surfaces are the following.

(1) The fully coordinated oxygen atoms always relax outward (i.e., toward the vacuum). Correspondingly, the T-shaped bonding structure (formed by each oxygen and its three neighboring Ti atoms), is distorted, and no longer planar. This behavior is observed for the (101), (100), and both (103) surfaces. On the $(103)_s$ surface, which has a fourfold-coordinated Ti atom, a remarkably large outward relaxation of the fully coordinated surface oxygen takes place. A distortion of the planar structure associated with a fully coordinated oxygen is also present on the (001) surface. This behavior can be rationalized in terms of the repulsion between oxygen atoms, as discussed for the bulk in Ref. 25.

TABLE VII. Structure of the ''smooth'' termination of the (103) surface. Atom labels refer to Fig. 7; also see the caption of Table III.

Atomic displacements (Å)				Bond expansion		
Label	[30$\bar{1}$]	[010]	(103)	Label	Type	%
O1	0.21	0.00	0.50	Ti1-O1	*e*	+0.6
O2	0.35	0.00	−0.06	Ti1-O2	*e*	−11.5
O3	0.11	0.00	−0.04	Ti1-O4	*a*	−8.4
O4	0.09	0.00	−0.05	Ti2-O1	*a*	+27.6
O5	0.10	0.00	0.12	Ti2-O3	*e*	−6.9
O6	0.09	0.00	−0.05	Ti2-O4	*e*	+2.8
O7	0.03	0.00	0.01	Ti2-O6	*a*	−9.2
O8	0.02	0.00	0.00	Ti2-O7	*e*	+4.6
				Ti3-O2	*e*	−0.9
Ti1	0.18	0.00	−0.20	Ti3-O3	*a*	−7.1
Ti2	0.31	0.00	−0.11	Ti3-O5	*e*	+0.2
Ti3	0.13	0.00	0.17	Ti3-O6	*e*	+7.2
				Ti3-O8	*a*	+3.4

TABLE VIII. Structure of the relaxed (110) surface. Atom labels refer to Fig. 8; also see the caption of Table III.

Atomic displacements (Å)				Bond expansion		
Label	[001]	[$\bar{1}$10]	(110)	Label	Type	%
O11	−0.19	0.35	0.23	Ti1-O11	*a*	−6.4
O12	0.29	0.09	−0.08	Ti1-O12	*a*	−9.3
O21	0.17	−0.32	0.23	Ti1-O21	*e*	−6.7
O22	0.05	−0.25	−0.37	Ti1-O22	*e*	−7.6
O31	0.09	0.02	0.05	Ti2-O11	*e*	−5.2
O32	0.05	0.05	0.02	Ti2-O12	*e*	−2.0
				Ti2-O21	*a*	+5.9
Ti1	0.08	−0.05	−0.37	Ti2-O22	*a*	+5.3
Ti2	0.07	−0.00	0.18	Ti2-O31	*e*	+4.1
Ti3	0.03	−0.03	−0.08	Ti2-O32	*e*	+7.6

(2) Bridging undercoordinated oxygens, forming with their neighbors a Ti-O-Ti δ angle, always relax so as to shorten the two Ti-O bond lengths by several percents. This is observed on the (101), (100), and both (103) surfaces.

(3) Bridging undercoordinated oxygens, forming with their neighbors a Ti-O-Ti θ angle, relax in such a way that the two O-Ti bonds, which are equivalent on the unrelaxed structure, become strongly inequivalent, one being substantially shorter than the other. This relaxation pattern is particularly evident on the (001) surface, and is likely related to the extremely high reactivity of this surface, which was observed in Ref. 7. The origin of this behavior is probably in the surface electronic structure, that we plan to analyze in detail in a future publication. From the bond lengths of the alternating short and long Ti-O bonds, however, we may speculate that these should have the character of double[36] and dative[7] bonds, respectively.

According to Burdett *et al.*,[13] the bulk structure of anatase is controlled by a balance between two forces: the O-O repulsions (which mainly determine the Ti-O bond distances and Ti-O-Ti bond angles) and the attractive Ti-O π interactions (which determine the planarity of the O-Ti_3 units). Our results for the anatase surfaces confirm this view: the O-O repulsions appear to be the most important factor in deciding the structure, and they are even able to destabilize the planar configuration of the surface oxygens, preferred on the basis of the π interactions. However, π interactions still have a significant role, as indicated by the symmetry breaking of the Ti-O bond lengths on the (001) surface.

V. CONCLUSIONS

We have presented an *ab initio* study of the bulk properties of TiO_2 in the phases of anatase and rutile, and an extensive study of many low-index anatase surfaces. Bulk properties were calculated with three different exchange-correlation functional [LDA,[14] PBE,[15] and BLYP (Ref. 16)]. Although we find that the anatase phase is slightly more stable than rutile, which is in disagreement with the experiment, we should remark that both the experimental [$\sim$1.2 kcal/mol (Ref. 21)] and calculated (see Table I) differences between the two phases is so small to be practically at the limit of accuracy of currently available DFT functionals. Thus, in spite of this shortcoming, the fact that the calculated structural parameters and elastic properties of both phases are in excellent agreement with the experiment provides a strong indication that surface relaxations are correctly described as well.

Low indexes anatase surfaces were studied with both LDA and PBE functionals. Although, as found previously for rutile surfaces,[28] the two approximations yield appreciably different surface energies, the relative stabilities of the different surfaces are the same, and atomic relaxation patterns are also very similar (which further supports their reliability). Thus, as it is possible to identify features in the atomic relaxations that are common to different surfaces, the surface energies also show general trends which are independent of the exchange-correlation functional. For instance, the (110) and $(103)_s$ surfaces, which have fourfold-coordinated Ti atoms, have a larger energy than those with fivefold-coordinated Ti atoms, and the surface energies of the relaxed structures approximately increase with the increase of the density of undercoordinated Ti atoms. Comparison with previous calculations[12] indicates that the average surface energy of an anatase crystal is lower than that of a crystal in the rutile phase. This could explain the fact that, experimentally, TiO_2 nanoparticles are found to prefer a less stable anatase structure for diameters up to about 10 nm.[11] The fact that surface energies play a crucial role in determining the nanoparticle structure is a further indication that the difference in stability between the anatase and rutile phases is indeed very small.

ACKNOWLEDGMENTS

The calculations of this work have been done at the Keck Materials Science Computing Center of the Princeton Materials Institute. We thank P. Giannozzi, N. Marzari, and S. Scandolo for helpful discussions.

[1] K. I. Hadjiivanov and D. G. Klissurski, Chem. Soc. Rev. **25**, 61 (1996).
[2] A. L. Linsebigler, G. Lu, and J. T. Yates, Chem. Rev. **95**, 735 (1995).
[3] B. O'Regan and M. Grätzel, Nature (London) **353**, 737 (1991); A. Hagfelt and M. Grätzel, Chem. Rev. **95**, 49 (1995).
[4] See, e.g., H. J. Freund, Faraday Discuss. **114**, 1 (1999).
[5] G. S. Herman, M. R. Sievers, and Y. Gao, Phys. Rev. Lett. **84**, 3354 (2000).
[6] R. Hengerer, P. Bolliger, M. Erbudak, and M. Grätzel, Surf. Sci. **400**, 162 (2000).
[7] A. Vittadini, A. Selloni, F. P. Rotzinger, and M. Grätzel, Phys. Rev. Lett. **81**, 2954 (1998).
[8] S. D. Burnside, V. Shklover, C. Barbé, P. Comte, F. Arendse, K. Brooks, and M. Grätzel, Chem. Mater. **10**, 2419 (1998).
[9] Y. Gao and S. A. Elder, Mater. Lett. **44**, 228 (2000).
[10] P. M. Oliver, G. W. Watson, E. T. Kelsey, and S. C. Parker, J. Mater. Chem. **7**, 563 (1997).
[11] H. Zhang and J. F. Banfield, J. Mater. Chem. **8**, 2073 (1998).
[12] M. Ramamoorthy, D. Vanderbilt, and R. D. King-Smith, Phys. Rev. B **49**, 16 721 (1994).
[13] J. K. Burdett, T. Hughbanks, G. J. Miller, J. W. Richardson, Jr., and J. V. Smith, J. Am. Chem. Soc. **109**, 3639 (1987).
[14] D. M. Ceperley and B. J. Alder, Phys. Rev. Lett. **45**, 566 (1980); J. P. Perdew and A. Zunger, Phys. Rev. B **23**, 5048 (1981).
[15] J. P. Perdew, K. Burke, and M. Ernzerhof, Phys. Rev. Lett. **77**, 3865 (1996).
[16] A. D. Becke, Phys. Rev. A **38**, 3098 (1988); C. Lee, W. Yang, and R. C. Parr, Phys. Rev. B **37**, 785 (1988).
[17] S. Kurth, J. P. Perdew, and P. Blaha, Int. J. Quantum Chem. **75**, 889 (1999).
[18] D. Vanderbilt, Phys. Rev. B **41**, 7892 (1990).

[19] F. D. Murnaghan, Proc. Natl. Acad. Sci. U.S.A. **30**, 244 (1944); F. Birch, J. Geophys. Res. **57**, 227 (1952).
[20] O. Gunnarsson, B. I. Lindqvist, and J. W. Wilkins, Phys. Rev. B **10**, 1319 (1974).
[21] *Handbook of Chemistry and Physics*, edited by R. C. West (CRC, Cleveland, 1986).
[22] *JANAF Thermochemical Tables*, 3rd ed. J. Phys. Chem. Ref. Data **14**, 1680 (1985).
[23] G. Cangiani, M. Posternak, and A. Baldereschi (unpublished) [M. Posternak (private communication)].
[24] J. K. Dewhurst and J. E. Lowther, Phys. Rev. B **54**, R3673 (1996).
[25] A. Fahmi, C. Minot, B. Silvi, and M. Causá, Phys. Rev. B **47**, 11 717 (1993).
[26] R. Colle and O. Salvetti, J. Chem. Phys. **79**, 1404 (1983).
[27] R. Car and M. Parrinello, Phys. Rev. Lett. **55**, 2741 (1985).
[28] J. Goniakowski, J. M. Holender, L. N. Kantorovich, M. J. Gillan, and J. A. White, Phys. Rev. B **53**, 957 (1996).
[29] Z. Yan, J. P. Perdew, S. Kurth, C. Fiolhais, and L. Almeida, Phys. Rev. B **61**, 2595 (2000).
[30] K. Carling, G. Wahnström, T. R. Mattsson, A. E. Mattsson, N. Sandberg, and G. Grimvall, Phys. Rev. Lett. **85**, 3862 (2000).
[31] L. Gerward and J. S. Olsen, J. Appl. Crystallogr. **30**, 259 (1997).
[32] J. Ziolkowski, Surf. Sci. **209**, 536 (1989).
[33] *CRC Handbook of Chemistry and Physics* 64th ed. (CRC, Boca Raton, FL, 1983).
[34] G. Wulff, Z. Kristallogr. Mineral. **34**, 449 (1901).
[35] T. Arlt, M. Bermejo, M. A. Blanco, L. Gerward, J. Z. Jiang, J. S. Olsen, and J. M. Recio, Phys. Rev. B **61**, 14 414 (2000).
[36] R. Guillard and C. Lecomte, Coord. Chem. Rev. **65**, 87 (1985).